Supporting Information

Size-dependent Inhibition of Herpesvirus Cellular Entry by Polyvalent Nanoarchitectures

Benjamin Ziem,[a] Walid Azab,[b] Mohammad FardinGholami,[c] Jürgen P. Rabe,[c] NikolausOsterrieder,[b]* and Rainer Haag[c]*

[a] Institute of Chemistry and Biochemistry, FreieUniversitätBerlin, 14195Berlin, Germany

[b]Institut für Virologie, Robert von Ostertag-Haus, Zentrum für Infektionsmedizin, Freie Universität Berlin, Robert-von-Ostertag-Str. 7-13, 14163 Berlin, Germany.

[c]Department of Physics & IRIS Adlershof, Humboldt-UniversitätBerlin, D-12489 Berlin, Germany

*

Content

1. Figures

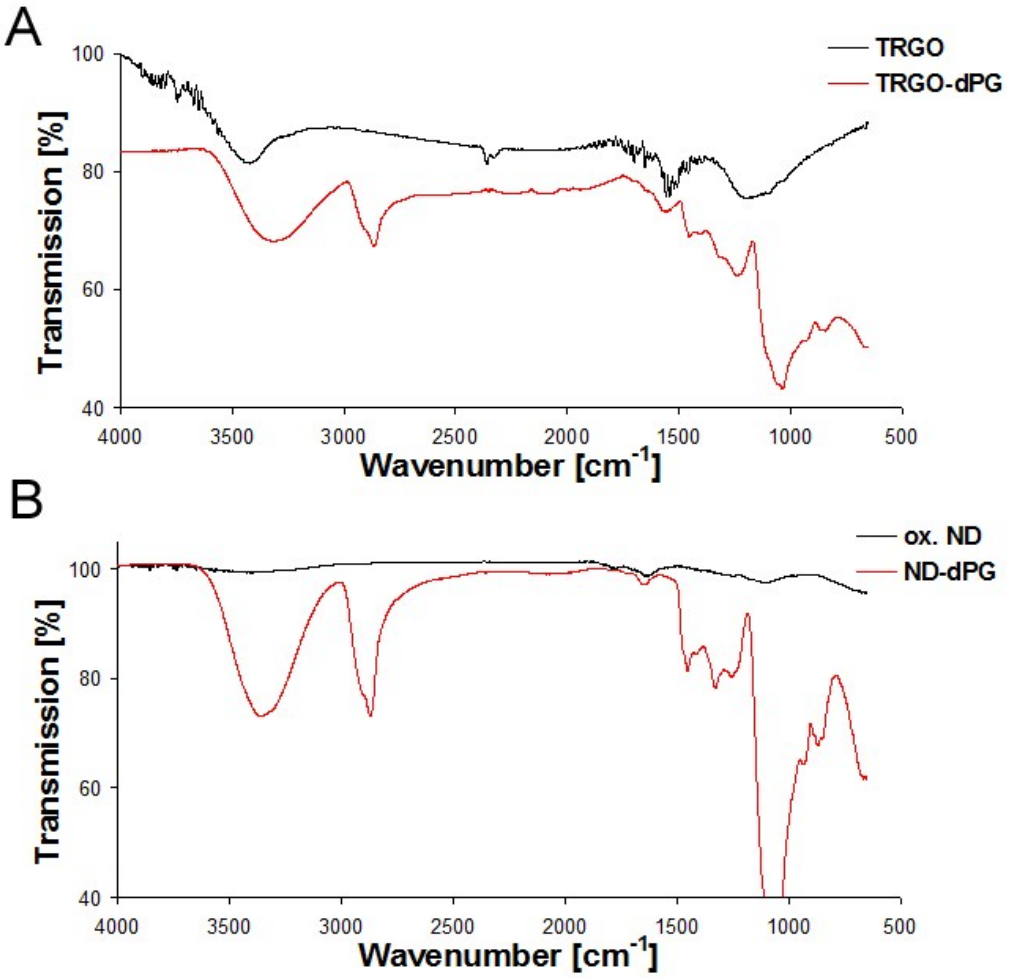

Figure S1. FTIR spectra of (A) TRGO and TRGO-dPG and (B) ox. ND and ND-dPG.

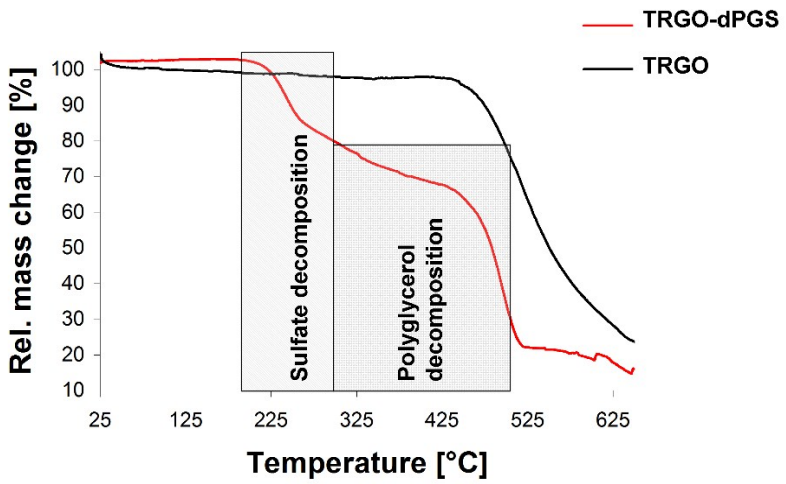

Figure S2. TGA curve comparison of TRGO-dPGS and TRGO.

2. Additional PRNT results

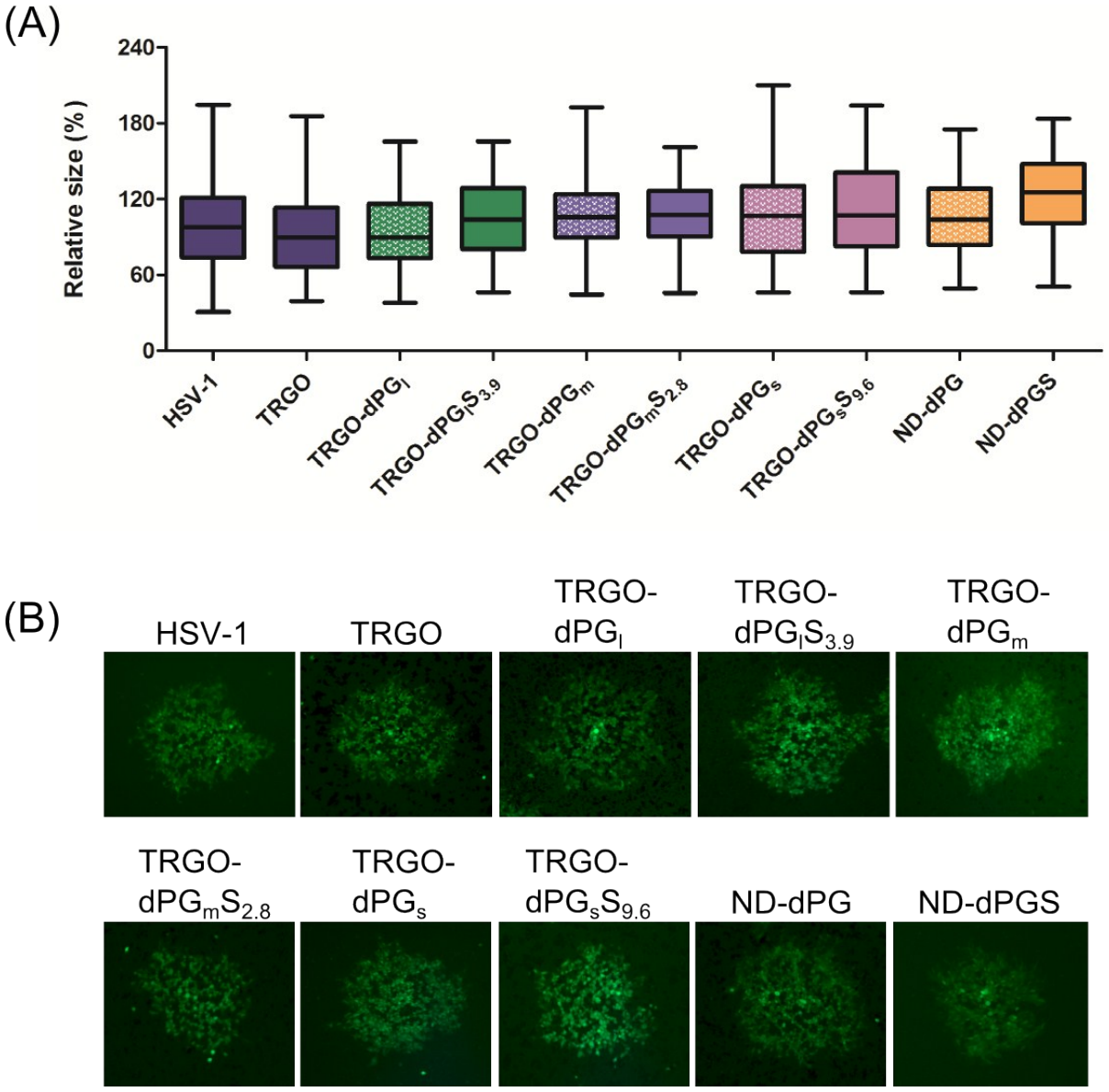

Figure S3. Determination of cell-to-cell spread by plaque size assay. (A) Vero cells were infected with HSV-1 at a MOI of 0.001 in the presence or absence of nanomaterials. After 72 h, 50 plaques were measured for each virus. The central line in the box plot indicates the median of the data, while the edges of the box indicate the 25th and 75th percentiles. Extending from the box are whiskers. The top whisker expands to the 95th percentile and the bottom whisker to the 5th percentile. The plaque diameter of parental viruses was set to 100%. (B) Plaques produced by GFP-expressing viruses. Pictures were taken using a Zeiss Axiovert fluorescence microscope.

3. Additional scanning force microscopy results

Wrapping of herpesvirus particles using functionalized graphene sheets

The functionalized thermally reduced graphene oxide (TRGO) sheets were spin casted from their deionized water dispersion onto the surface of a freshly cleaved highly oriented pyrolytic graphite (HOPG, ZYA, Momentive Performance) at a casting time of 10 minutes and speed of 40 rps for 2 minutes. Scanning force microscopy in tapping and quantitative modes were carried out on the prepared samples using a Nanowizard 3 (JPK, GmbH) instrument. The Nanowizard 3 instrument was operated in Quantitative Imaging mode (QI) at atypical rate of 10-17 min per image and an image resolution of 128x128 pixels. The contact, i.e. zero force, point on extent curves in QI mode was assigned to be topography. Silicon tips on silicon nitride cantilevers with a tetrahedral base were used with a typical resonance frequency of 70 kHz and spring constant of 1.7 to 2 N/m (OLTESPA-R3). The tips exhibited a typical apex radius of 7 nm with an upper limit of 10 nm, having a tip cone half angle of 18 degrees, as specified by the manufacturer (Bruker Corporation). Experiments were carried out under ambient conditions. Deflection sensitivity was calibrated by acquiring force-distance curves on a sapphire surface (Bruker Corporation). Cantilever spring constants were calibrated using the thermal noise method.[1] Set points in the range of 1 nN to 7 nN were used. The TM-SFM images were processed and analyzed with SPIP (Image Metrology A/S) and JPK image processing software. Topography images were line flattened with first order polynomial. For reference experiments, a 20 μL droplet of phosphate buffer solution (PBS) was placed onto the HOPG surface accommodating the functionalized sheets and then, the SFM scanning was carried out in liquid (PBS buffer).

Furthermore, experiments including both the functionalized TRGO and herpes virions were carried out by first deposition of the sheets onto a freshly cleaved HOPG surface and then addition of 5 μL droplet of the herpesvirus in PBS buffer solution with 15 μL of excess PBS buffer to create a 20 μL droplet on the surface of the HOPG containing functionalized

sheets. Afterwards, scanning force microscopy in quantitative imaging mode was carried out to investigate the interaction of the functionalized TRGO sheets with herpes virions.

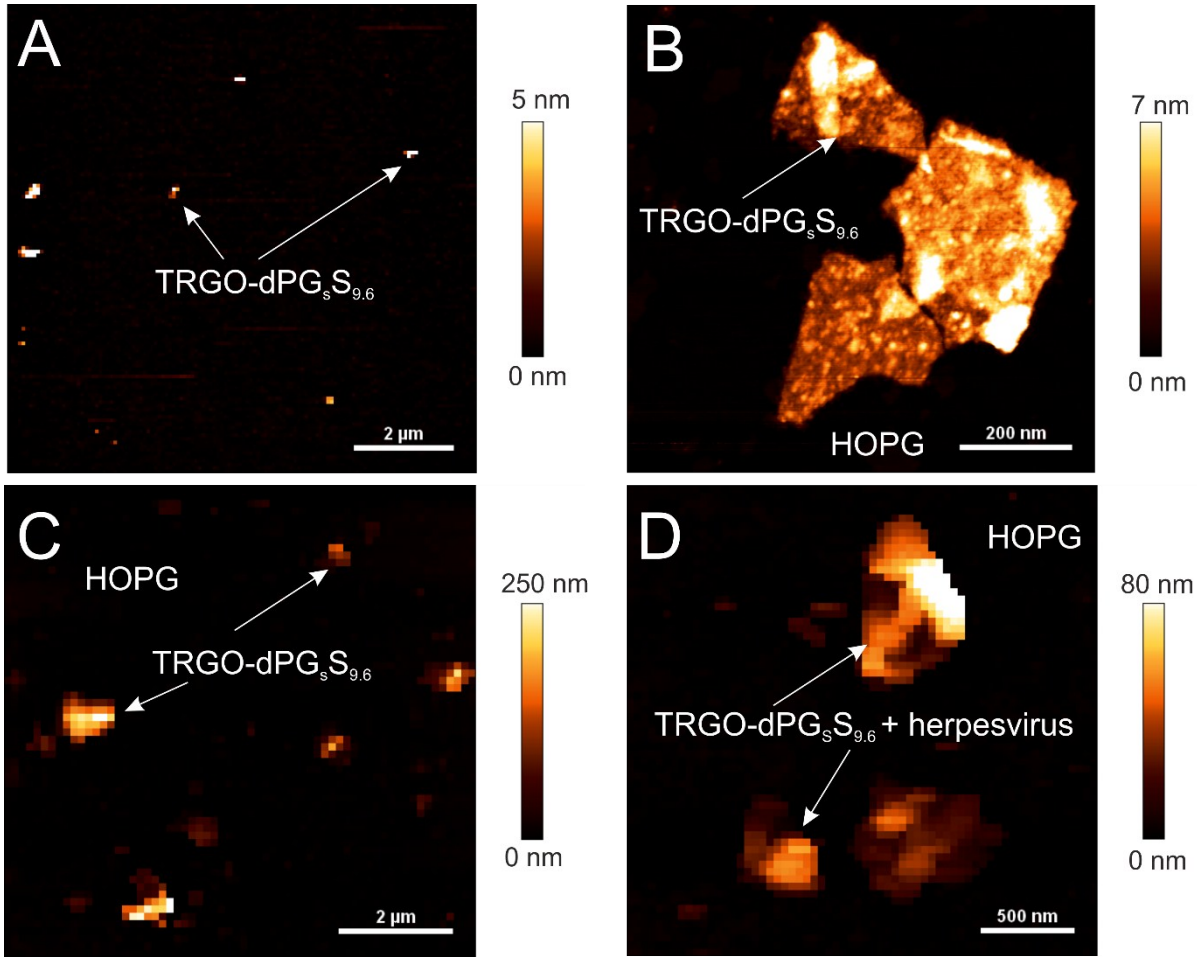

Figure S4. (A) Large scan area (88 µm^2) of functionalized TRGO sheets deposited onto the HOPG surface from water dispersion (Measurement in ambient). (B) Close up of the functionalized TRGO sheets of small size with their typical heights with open but wrinkled morphology containing spherical hyperbranched polyglycerols. (C) Large scan area (100 µm^2) of the functionalized TRGO sheets forming large aggregates (sacks) around the virions in a 20 µL PBS buffer solution (Measurement in liquid). (D) Typical geometries and heights of the aggregates (sacks) of functionalized TRGO sheets containing virion.

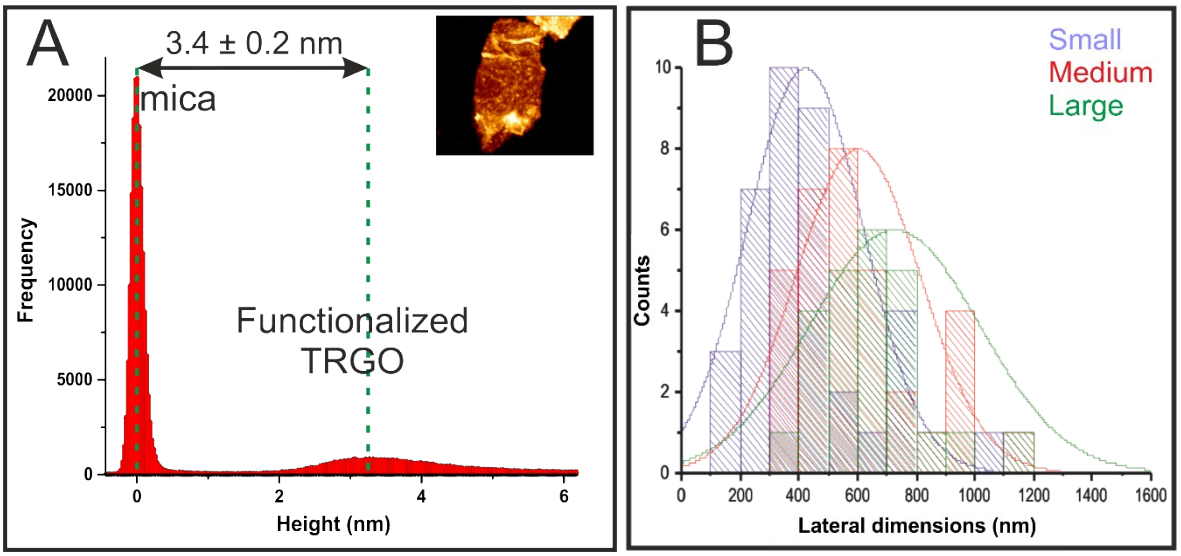

Figure S5. (A) Histogram analysis of the height of a typical single layer TRGO-dPG sheet shown as inset when deposited from solution onto a freshly cleaved mica surface fitted with two Gaussian functions shown in red. (B) Histogram analysis of the lateral dimensions of the TRGO-dPG sheets of three main variations of small, medium and large. Individual data sets are fitted with a Gaussian function shown in purple, red and green.

The number of the aggregates (sacks of virion) formed in a 100 μm^2 area of the HOPG surface directly depends on the concentration of the functionalized TRGO in the DI water dispersion. It was possible to observe up to 7 Sacks of virion formed as a result of incubation of the virions in PBS buffer on top of the HOPG coated with functionalized TRGO sheets. Furthermore, the area, diameter and the material volume of the sacks of virions imaged using SFM-QI mode were measured using the height based pixel filtration of the SFM-QI images as explained in the previous study.[2]

Figure S6 represents the histogram on the distribution of the diameter, material volume and area of the sacks of virion formed during *in situ* scanning of the functionalized sheets with herpesvirus dispersed in PBS buffer.

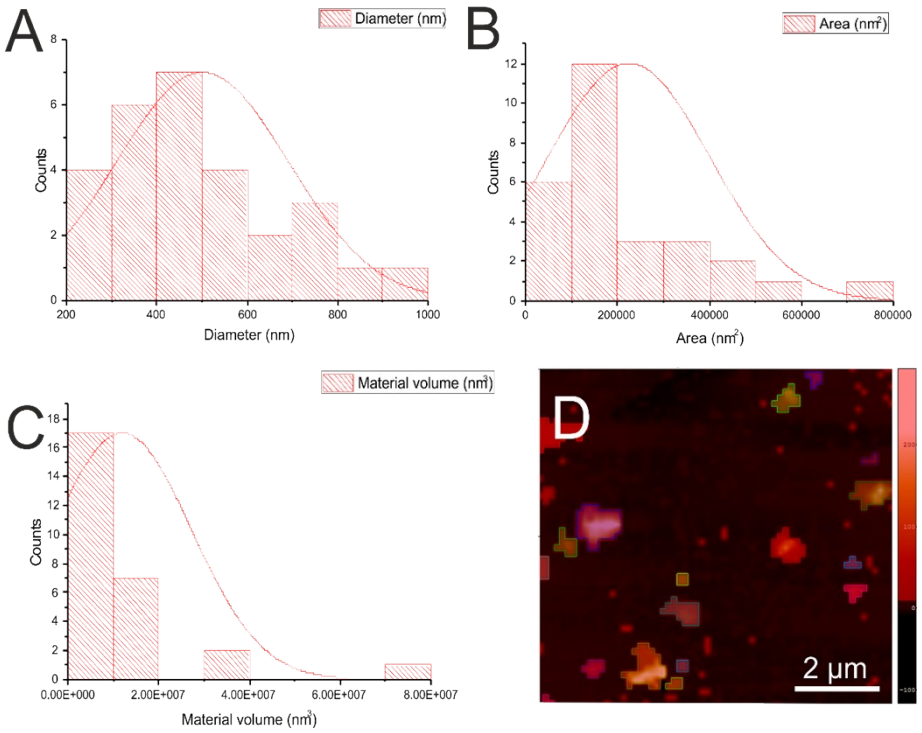

Figure S6. (A) Histogram of distribution of the diameter of aggregates attributed to the sacks of virion. (B) Histogram of distribution of the area of aggregates attributed to the sacks of virion. (C) Histogram of distribution of the volume of aggregates attributed to the sacks of virion. (D) An example of the height based pixel filtration of the SFM-QI images used to calculate the diameter, area and material volume.

Figure S7 shows the state of the functionalized TRGO sheets deposited on to the HOPG surface and scanned in liquid (PBS buffer) droplet.

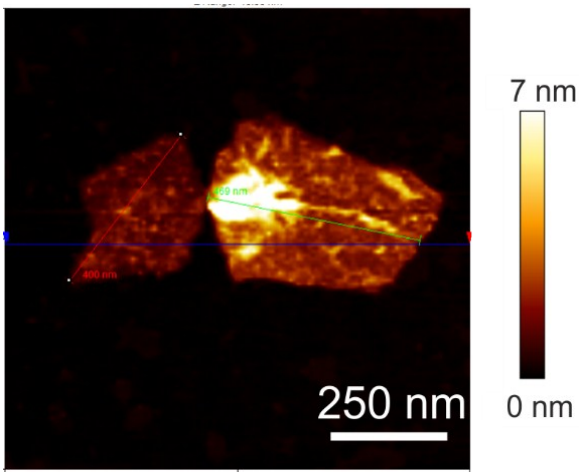

Figure S7. SFM-QI mode image of the functionalized TRGO sheet on top of the HOPG surface, as imaged in PBS buffer droplet in liquid conditions.

Figure S8 indicates the stiffness map of the sacks of virion formed during SFM-QI imaging of the HOPG coated with functionalized TRGO sheets immersed in a droplet of herpesvirus dispersed in PBS buffer (Measurement in liquid). Figures S8A, S8B show the stiffness difference by variation of the slope of the extend curves in force spectra extracted form QI imaging mode. Using JPK image processing software, the extracted slope value is plotted as a map and therefore, a stiffness map is made Figure S8C.

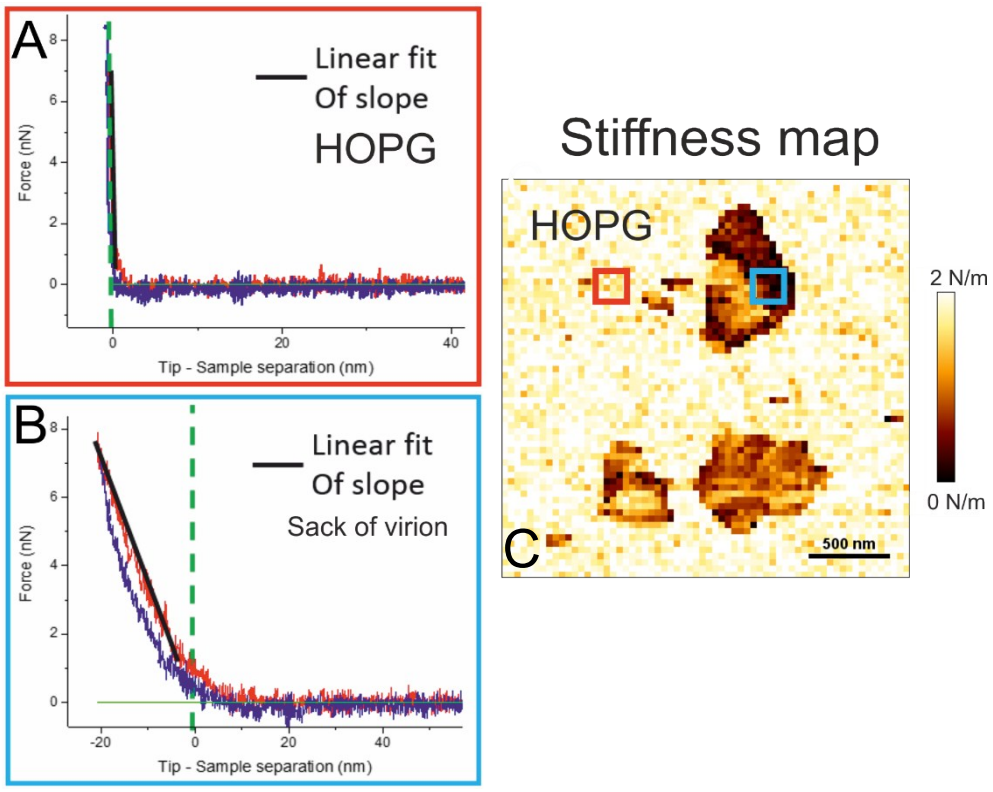

Figure S8. (A) The force spectra extracted from quantitative imaging of the sample in liquid (PBS) (red square in Figure S8C) over HOPG shows a very steep slope of extend and retract curves which is fitted with a line. (B) The force spectra extracted from quantitative imaging of the sample in liquid (PBS) over the sack of virion (blue square in Figure S8C). (C) Stiffness map plotted based on the value of Extend curve slope extracted from every pixel of the QI imaging mode.

4. Dynamic light scattering results

Dynamic light scattering was used to evaluate the size dimensions of the free HSV-1 particles, the polyvalent nanoarchitectures, and the mixture of both of them. In this context, it turns out that the average size dimensions of the medium (630 ± 26 nm) and largest (1004 ± 72 nm) graphene sheets are decreased in the presence of HSV-1 particles (203 ± 17 nm) to the following values: medium sheet = (411 ± 81 nm) and large sheets = (823 ± 64nm)

In the case of the smallest functionalized sheets (391 ± 48 nm) an increase in size was detected (699 ± 77 nm) which is consistent with the SFM results.

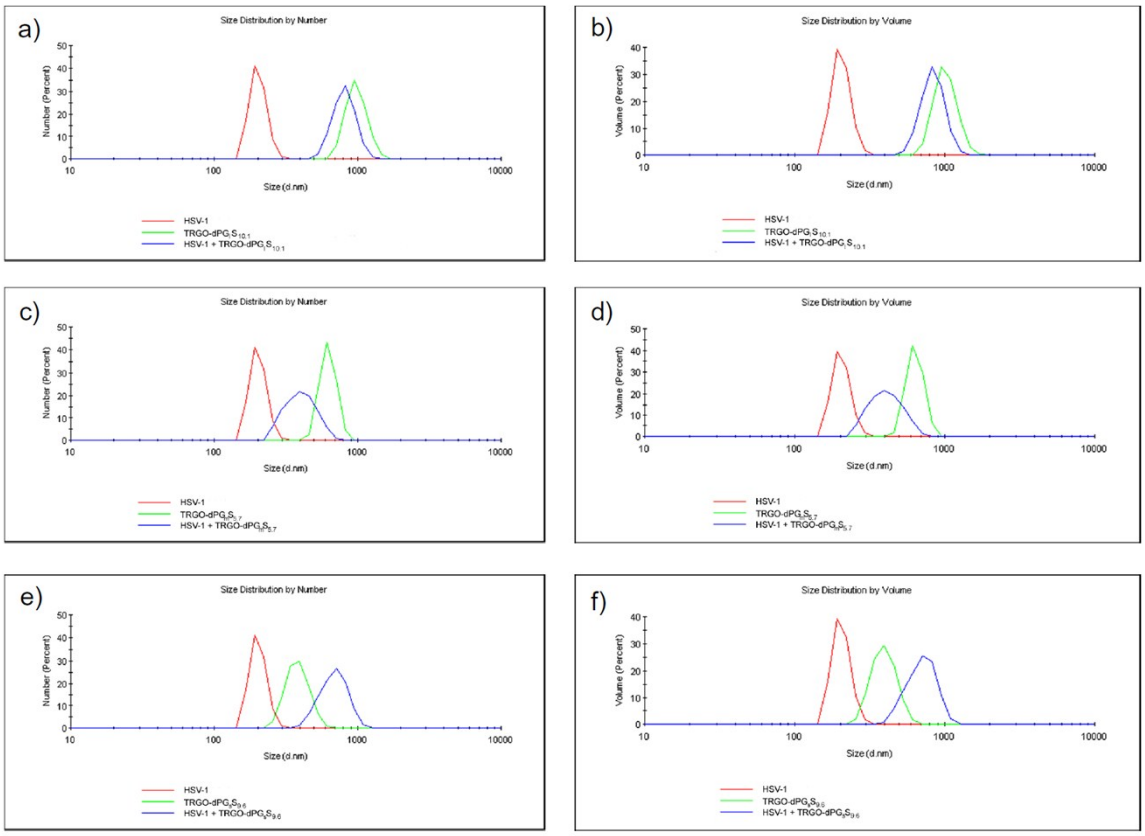

Figure S9. Size distribution measurements by using dynamic light scattering in PBS. Comparison of the average size distributions by number for (a) HSV-1 (red), TRGO-dPG$_l$S$_{10.1}$ + HSV-1 (blue), and TRGO-dPG$_l$S$_{10.1}$ (green), (c) HSV-1 (red), TRGO-dPG$_m$S$_{5.7}$ + HSV-1 (blue), and TRGO-dPG$_s$S$_{9.6}$ (green), and (e) HSV-1 (red), TRGO-dPG$_s$S$_{9.6}$ + HSV-1 (blue). Comparison of the average size distributions by volume for (b) HSV-1 (red), TRGO-dPG$_l$S$_{10.1}$ + HSV-1 (blue), and TRGO-dPG$_l$S$_{10.1}$ (green), (d) HSV-1 (red), TRGO-dPG$_m$S$_{5.7}$ + HSV-1 (blue), and TRGO-dPG$_s$S$_{9.6}$ (green), and (f) HSV-1 (red), TRGO-dPG$_s$S$_{9.6}$ + HSV-1 (blue).

5. Additional Procedures and Characterizations

5.1. Preparation and characterization of graphite oxide

The graphite oxide (GO) was produced according to a modified Hummers and Offeman oxidation protocol.[3-5] Briefly, prisitne graphite (60 g) was oxidized at room temperature in a mixture of concentrated H_2SO_4 (95%, 1.4 L) and $NaNO_3$ (30 g) followed by a portion wise addition of $KMnO_4$ (180 g) at 0°C over a period of 5 h. The oxidation process was quenched in ice water after 2 days and then treated with H_2O_2 (3%, 200 mL). The produced GO was filtered off and washed at least 10 times before drying for 4 days. To pulverize the final product a CyroMill (60 µm mesh) was used. IR: 3417 cm^{-1} (ν, O-H), 1714 cm^{-1} (ν, C=O), 1556 cm^{-1} (ν, C=C), 1454 cm^{-1} (δ, C-H), 1225–1134 cm^{-1} (ν, C-O), 1067 cm^{-1} (δ, O-H), 941 cm^{-1} (δ, C=C); EA: C: 57.0%, H: 2.6%, O*: 40.4% (*calculated based on the CHN-values).

5.2. Preparation and characterization of thermally reduced graphene oxide

Thermally reduced graphene oxide (TRGO) was prepared according to a published procedure.[3,4] To enhance the exfoliation process of graphene, graphite oxide (50 g) was thermally reduced in a tube furnace under inert conditions at 400°C. Due to this method mono- and few-layer graphenes were produced and continuedto be processed without further purification. IR: 3417 cm^{-1} (ν, O-H), 1714 cm^{-1} (ν, C=O), 1556 cm^{-1} (ν, C=C), 1454 cm^{-1} (δ, C-H), 1225–1134 cm^{-1} (ν, C-O), 1067 cm^{-1} (δ, O-H), 941 cm^{-1} (δ, C=C); EA: C: 80.9%, H: 1.2%, O*: 17.9% (*calculated based on the CHN-values).

5.3. Characterizationof TRGO-polyglycerol

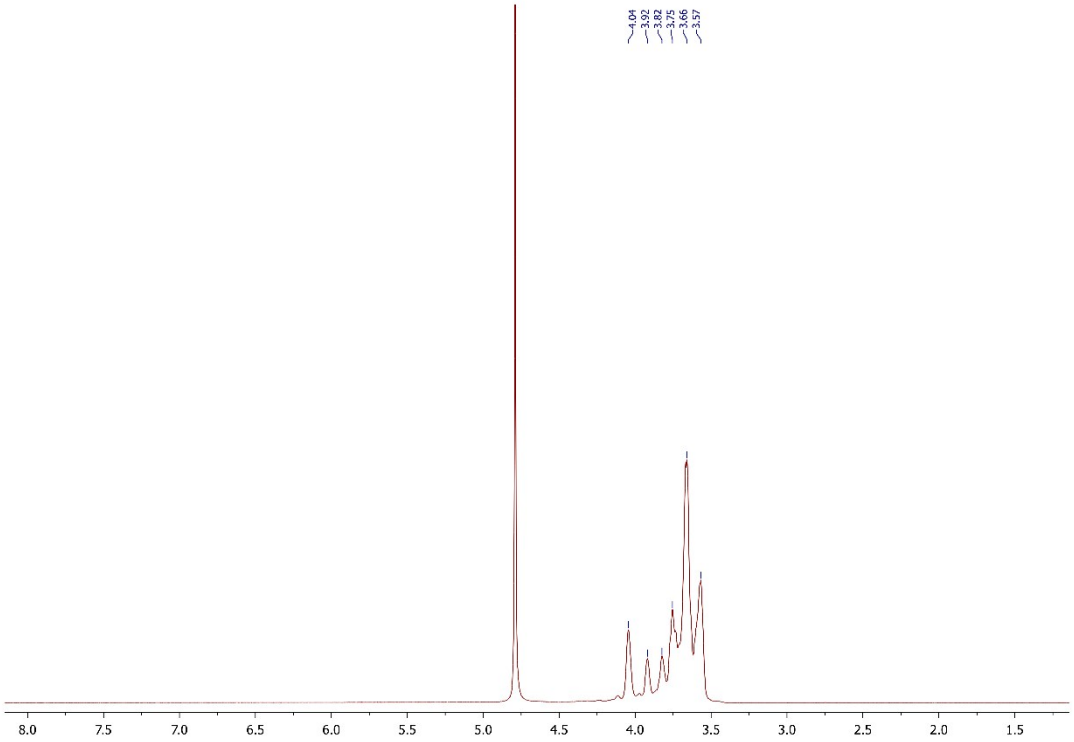

Figure S10. ^{1}H NMR spectra of TRGO-dPG$_{l}$.

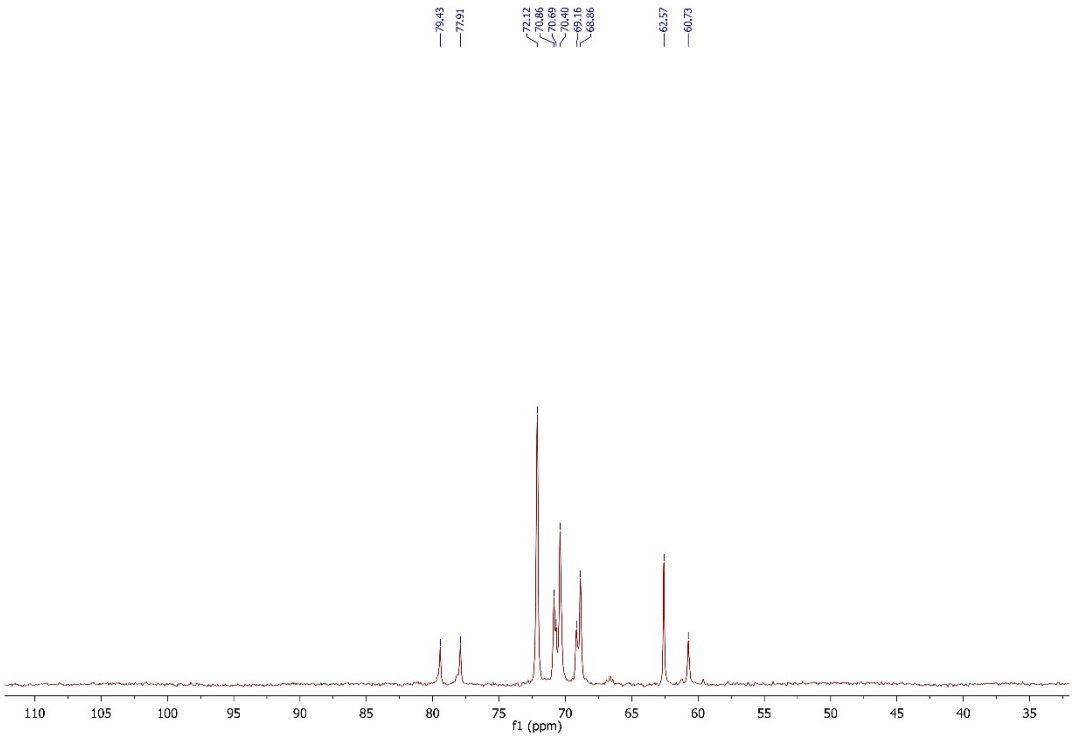

Figure S11. ^{13}C NMR spectra of TRGO-dPG$_{l}$.

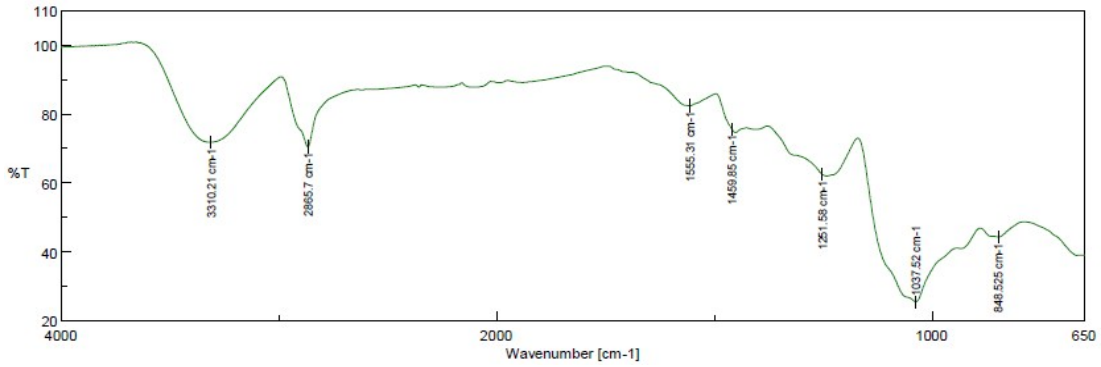

Figure S12. FTIR spectra of TRGO-dPG$_l$.

5.4. Characterization of TRGO-polyglycerol sulfate derivatives

Synthesis of the TRGO-polyglycerol sulfate derivatives (TRGO-dPG$_x$S$_y$**)** (**x**: represents large (l), medium (m), small (s) mean surface area of the graphene sheet and **y**:describes the degree of sulfation of the polymerized surface). In short, TRGO-dPG$_x$ (35 - 50 mg) was dispersed in dry DMF (8 - 10 mL) by continuous sonication for 60 min under argon atmosphere. Afterwards the dispersion was heated up to 60 °C and a dropwise addition of the sulfur trioxide pyridine complex (0.9 - 128.9 mg) dissolved in dry DMF (2 mL) was initiated. The reaction was kept at 60 °C for additional 24 h and then quenched with distilled water (20 mL) at room temperature. Through addition of dissolved sodium hydroxide the pH was adjusted to 8 before precipitating the TRGO-dPG$_x$S$_y$ by using a centrifuge (5 times at 8850 g, 30 min). The final product was dialyzed for 3 days in distilled water to remove the remaining DMF.

Table S1 Required amounts of educts and solvent to synthesize the targeted TRGO-dPG$_x$S$_y$ derivative.

Products\ Educts	TRGO-dPG$_l$	TRGO-dPG$_m$	TRGO-dPG$_s$	Sulfur trioxide pyridine complex	DMF
TRGO-dPG$_l$S$_{10.1}$	50.0 mg	—	—	128.9 mg	10.0 mL
TRGO-dPG$_l$S$_{3.9}$	50.0 mg	—	—	12.9 mg	9.0 mL
TRGO-dPG$_l$S$_{1.0}$	50.0 mg	—	—	1.3 mg	8.0 mL
TRGO-dPG$_m$S$_{5.7}$	—	35.0 mg	—	45.1 mg	10.0 mL
TRGO-dPG$_m$S$_{2.8}$	—	35.0 mg	—	9.0 mg	9.0 mL
TRGO-dPG$_m$S$_{1.6}$	—	35.0 mg	—	0.9	8.0 mL
TRGO-dPG$_s$S$_{9.6}$	—	—	35.0 mg	90.2 mg	10.0 mL
TRGO-dPG$_s$S$_{2.2}$	—	—	35.0 mg	9.0 mg	9.0 mL
TRGO-dPG$_s$S$_{1.3}$	—	—	35.0 mg	0.9	8.0 mL

Characterization on the example of TRGO-dPG$_l$S$_{10.1}$

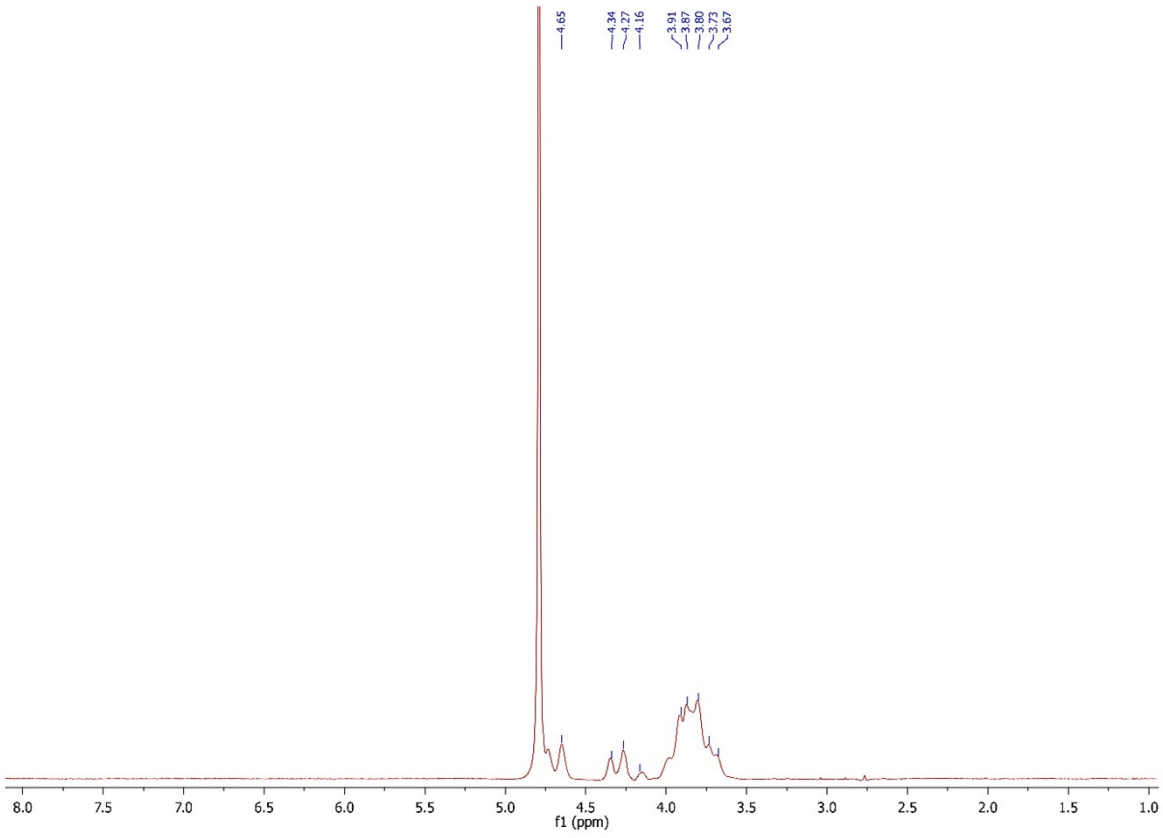

Figure S13. ^{1}H NMR spectra of TRGO-dPG$_l$S$_{10.1.}$

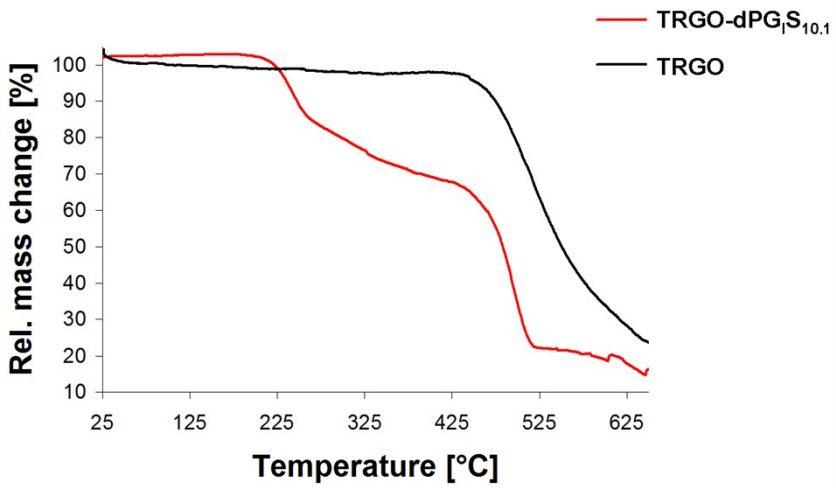

Figure S14. TGA spectra ofTRGO-dPG$_l$S$_{10.1}$ and TRGO.

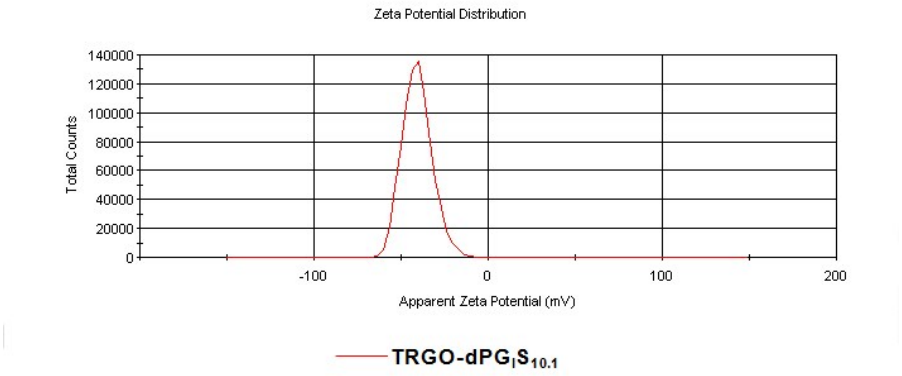

Figure S15. Average zeta potential ofTRGO-dPG$_l$S$_{10.1.}$

TRGO-dPG$_l$S$_{3.9}$

^{1}H NMR (700 MHz, D_2O) δ (ppm) 4.02–3.62 (m, broad, PG); EA: C: 66.9%, H: 4.2%, N: 0.5%, S: 1.5%, O*: 26.9% (*calculated based on the CHNS-values); TGA: 22% TRGO and 78% dPGS; DS: 3.9%; ζ Zeta Potential:-32.4 mV.

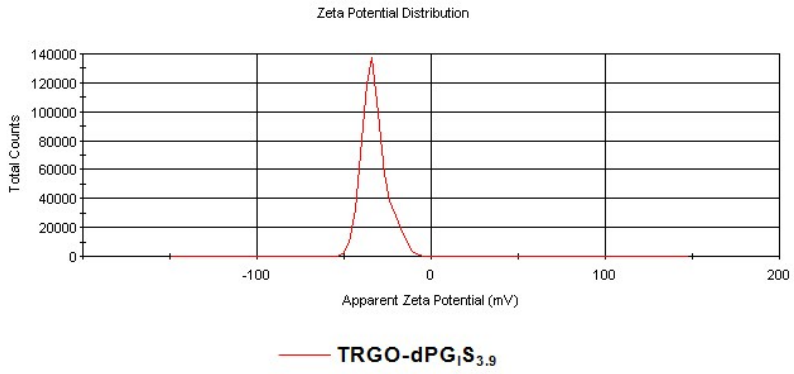

Figure S16. Average zeta potential of TRGO-dPG$_l$S$_{3.9}$.

TRGO-dPG$_l$S$_{1.0}$

^{1}H NMR (700 MHz, D_2O) δ (ppm) 4.05–3.59 (m, broad, PG); EA: C: 66.9%, H: 4.2%, N: 0.5%, S: 1.5%, O*: 26.9% (*calculated based on the CHNS-values); TGA: 18% TRGO and 82% dPGS; DS: 1.0%; ζ Zeta potential:-22.1 mV.

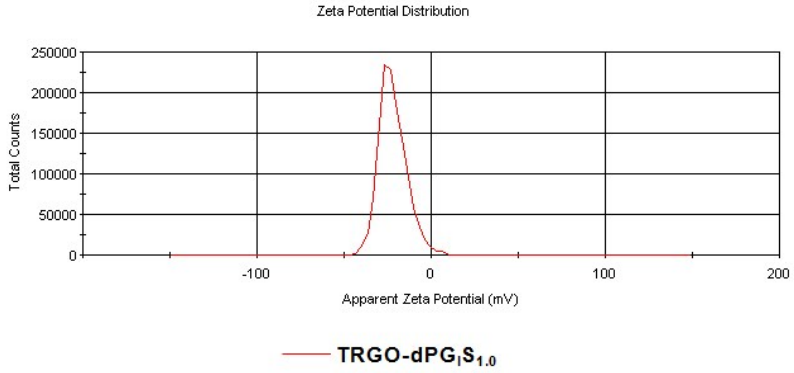

Figure S17. Average zeta potential of TRGO-dPG$_l$S$_{1.0}$.

TRGO-dPG$_m$S$_{5.7}$

^{1}H NMR (700 MHz, D_2O) δ (ppm) 4.03–3.61 (m, broad, PG); EA: C: 65.9%, H: 3.8%, N: 0.3%, S: 1.9%, O*: 28.1% (*calculated based on the CHNS-values); TGA: 17% TRGO and 83% dPGS; DS: 5.7%; ζ Zeta potential:-35.2 mV.

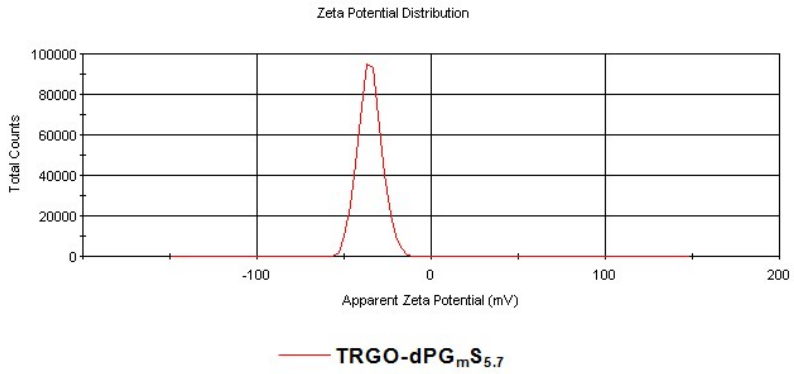

Figure S18. Average zeta potential of TRGO-dPG$_m$S$_{5.7}$.

TRGO-dPG$_m$S$_{2.8}$

^{1}H NMR (700 MHz, D_2O) δ (ppm) 4.04–3.58 (m, broad, PG); EA: C: 69.2%, H: 4.1%, N: 0.4%, S: 1.0%, O*: 25.3% (*calculated based on the CHNS-values); TGA: 18% TRGO and 82% dPGS; DS: 2.8%; ζ Zeta potential:-31.2 mV.

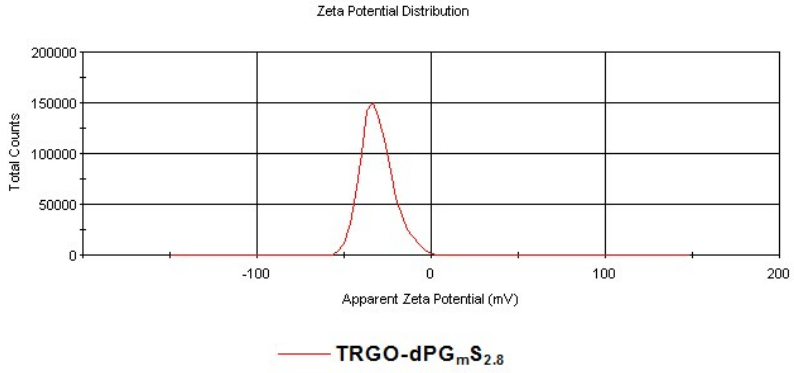

Figure S19. Average zeta potential of TRGO-dPG$_m$S$_{2.8}$.

TRGO-dPG$_m$S$_{1.6}$

^{1}H NMR (700 MHz, D_2O) δ (ppm) 4.02–3.58 (m, broad, PG); EA: C: 68.3%, H: 4.2%, N: 0.4%, S: 0.6%, O*: 27.4% (*calculated based on the CHNS-values); TGA: 18% TRGO and 82% dPGS; DS: 1.6%; ζ Zeta potential:-22.7 mV.

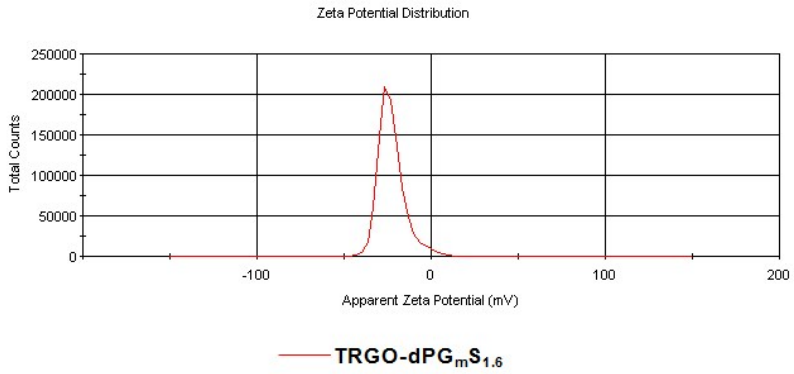

Figure S20. Average zeta potential of TRGO-dPG$_m$S$_{1.6}$.

TRGO-dPG$_s$S$_{9.6}$

^{1}H NMR (700 MHz, D_2O) δ (ppm) 4.04–3.59 (m, broad, PG); EA: C: 61.7%, H: 4.1%, N: 0.5%, S: 3.4%, O*: 30.3% (*calculated based on the CHNS-values); TGA: 25% TRGO and 75% dPGS; DS: 9.6%; ζ Zeta potential:-39.4 mV.

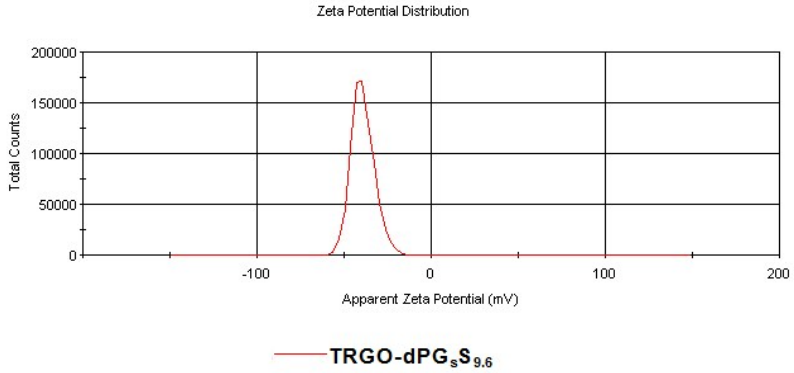

Figure S21. Average zeta potential of TRGO-dPG$_s$S$_{9.6}$.

TRGO-dPG$_s$S$_{2.2}$

^{1}H NMR (700 MHz, D_2O) δ (ppm) 4.05–3.62 (m, broad, PG); EA: C: 63.2%, H: 4.1%, N: 0.3%, S: 0.6%, O*: 31.8% (*calculated based on the CHNS-values); TGA: 22% TRGO and 78% dPGS; DS: 2.2%; ζ Zeta potential:-27.7 mV.

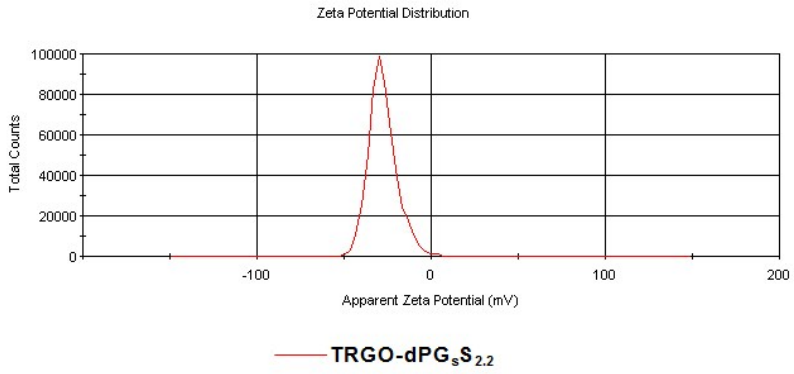

Figure S22. Average zeta potential of TRGO-dPG$_s$S$_{2.2}$.

TRGO-dPG$_s$S$_{1.3}$

^{1}H NMR (700 MHz, D_2O) δ (ppm) 4.02–3.62 (m, broad, PG); EA: C: 67.2%, H: 3.8%, N: 0.3%, S: 0.3%, O*: 28.4% (*calculated based on the CHNS-values); TGA: 22% TRGO and 78% dPGS; DS: 1.3%; ζ Zeta potential:-22.9 mV.

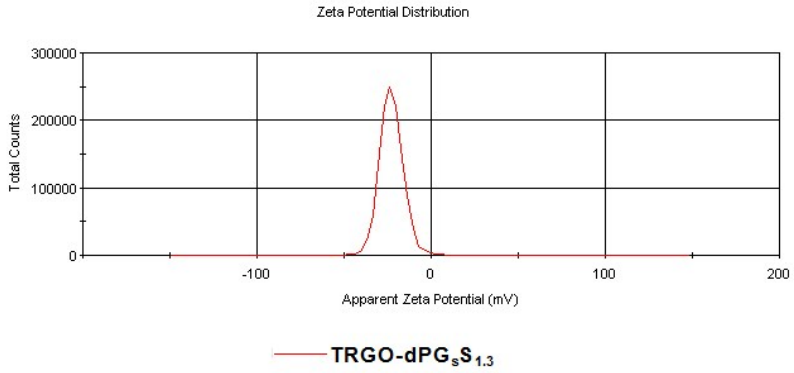

Figure S23. Average zeta potential of TRGO-dPG$_s$S$_{1.3}$.

5.5. Preparation and characterization of oxidized nanodiamonds:

The nanodiamonds have been oxidized based on the method reported by Haag et al.[6] In short, pristine nanodiamonds (0.50 g) have been dispersed by sonication in a 3:1 mixture of conc. sulfuric acid (96%, 24 mL) and nitric acid (65%, 8 mL). The stable dispersion was heated up to 80 °C for 9 h before cooling down to room temperature. Afterwards the dispersion was

iteratively diluted with distilled water and then centrifuged 10 times (8850 g, 30 min) until a neutral pH was adjusted. The precipitates were collected and dialyzed for 3 days in distilled water for further purification. IR: 3406 cm^{-1} (v, O-H), 1773 cm^{-1} (v, C=O), 1636 cm^{-1} (v, C=O), 1250 cm^{-1} (v, C-O), 1105 cm^{-1} (δ, O-H); EA: C: 79.3%, H: 1.3%, N: 2.6% O*: 16.8% (*calculatedbasedonthe CHNvalues).

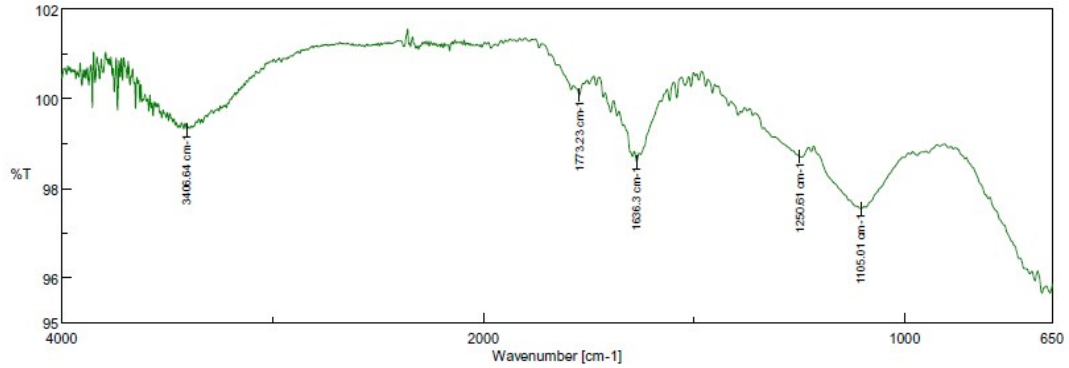

Figure S24. FTIR spectra of the oxidized nanodiamond.

5.6. Characterization of ND-polyglycerol

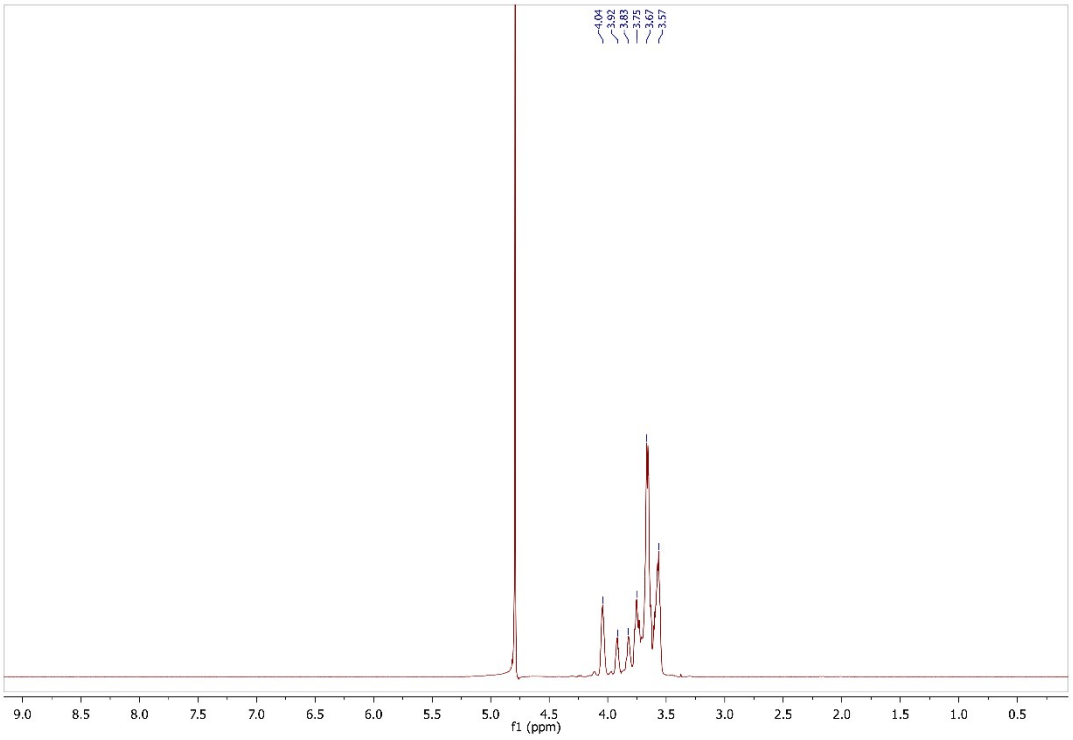

Figure S25. ^{1}H NMR spectra of ND-dPG.

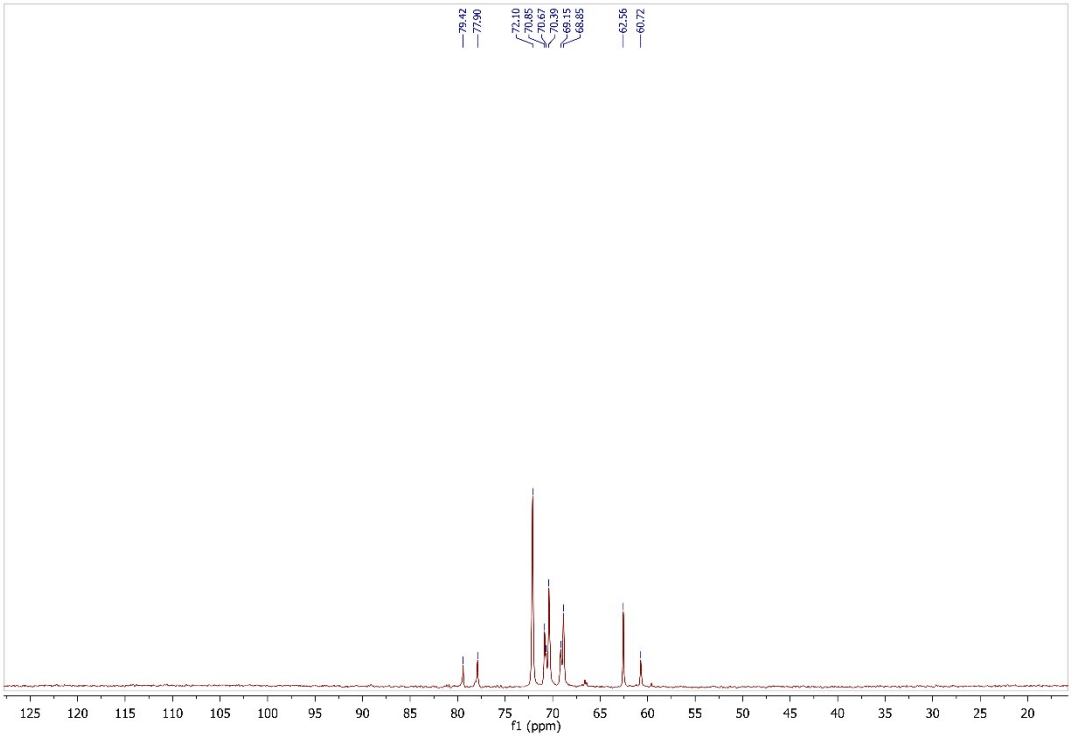

Figure S26. ^{13}C NMR spectra of ND-dPG.

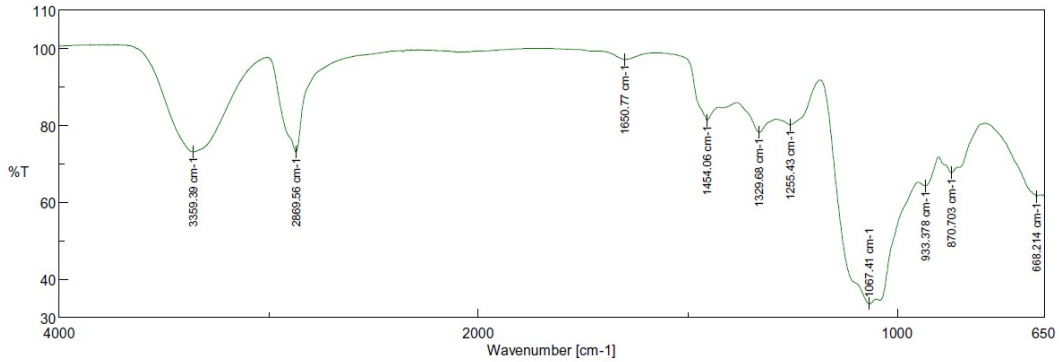

Figure S27. FTIR spectra of ND-dPG.

5.7. Characterization of ND-polyglycerol sulfate

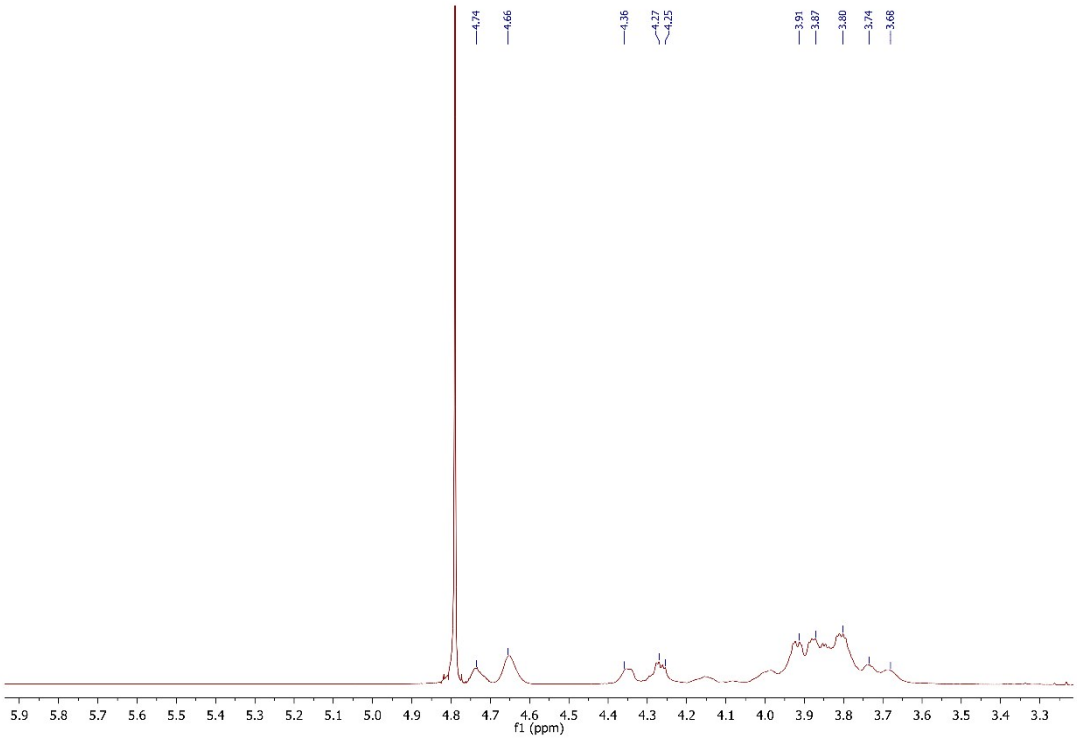

Figure S28. ^{1}H NMR spectra of ND-dPGS.

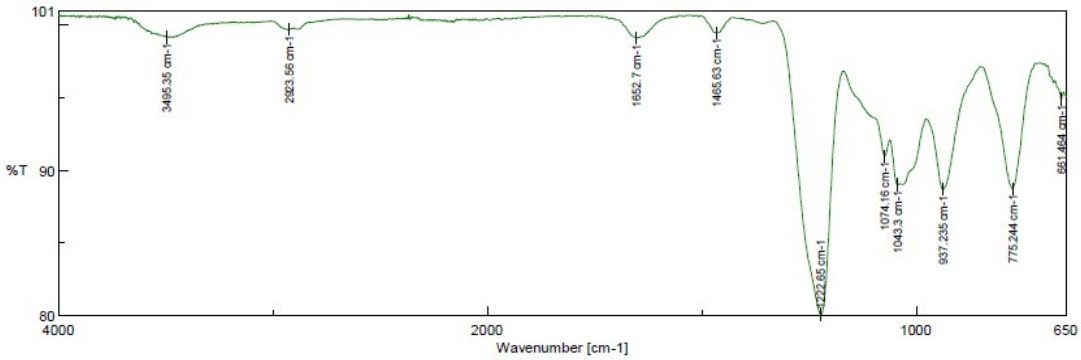

Figure S29. FTIR spectra of ND-dPGS.

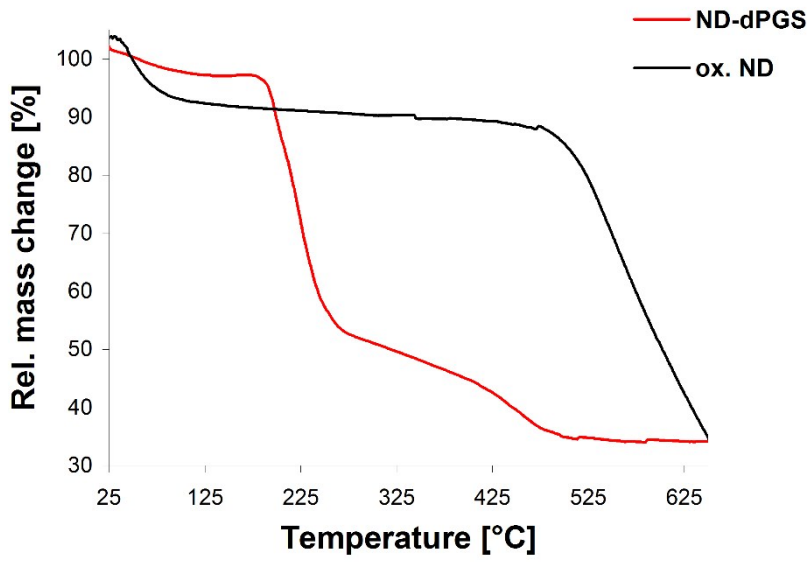

Figure S30. TGA curveof ND-dPGS and ox. ND.

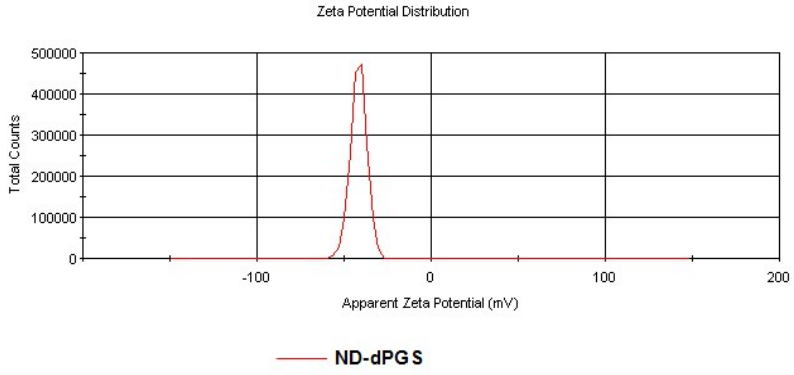

Figure S31. Average zeta potential of ND-dPGS

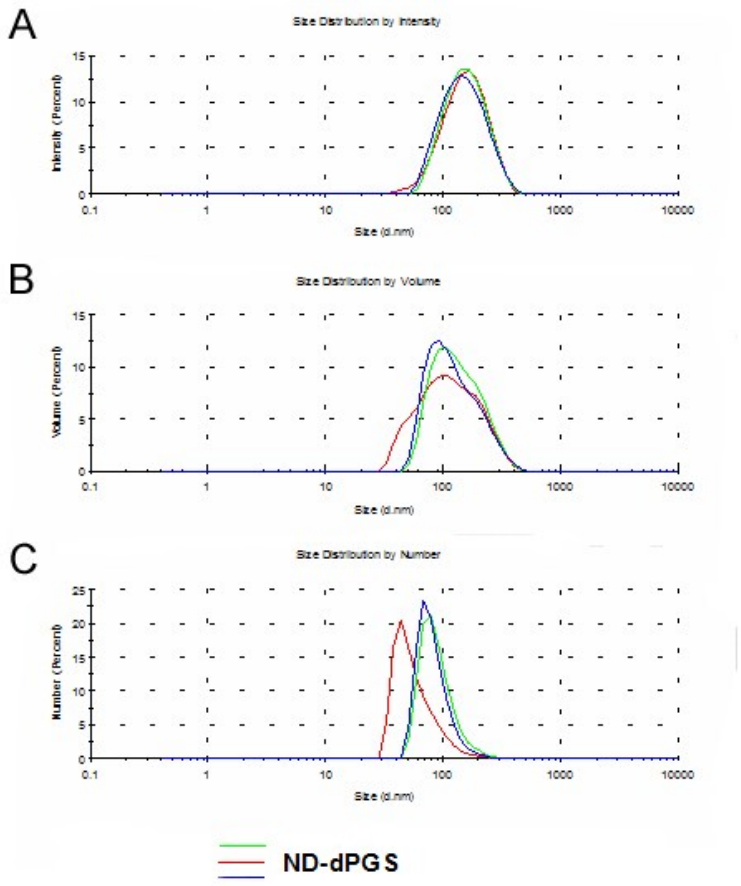

Figure S32. Size distribution measurement of ND-dPGS by (A) intensity, (B) volume and (C) number.

6. Additional References

1 H. J. Butt and M. Jaschke. M, *Nanotechnology,* 1995, **6,** 1-7.

2 B. Ziem, H. Thien, K. Achazi, C. Yue, D. Stern, K. Silberreis, M. F. Gholami, F. Beckert, D. Gröger, R. Mülhaupt, J. P. Rabe, A. Nitsche, R. Haag, *Adv. Healthc. Mater.,* **2016**, DOI:10.1002/adhm.201600812

3 F. J. Tolle, M. Fabritius and R. Mülhaupt, *Adv. Funct. Mater.,*2012, **22**, 1136.

4 K. Appel, R. Thomann and R. Mülhaupt, *Polymer,*2012, **53**, 4931.

5 W. S. Hummers and R. E. Offeman, *J. Am. Chem. Soc.,*1958, **80**, 1339.

6 M. C. Lukowiak, B. Ziem, K. Achazi, G. Gunkel-Grabole, C. S. Popeney, B. N. S. Thota, C. Böttcher, A. Krueger, Z. Guan and R. Haag, *J. Mater. Chem. B,* 2015, **3**, 719-722.